Data Repository File DR1. Expanded Methods & Supplemental Figures

This supplementary file provides expanded details regarding the methodology (sample preparation, U-Pb analytical methods, data reduction, age determinations) and supplemental Figures DR1–DR6. It should be cited as the paper it accompanies:

> Darin, M.H., Armentrout, J.M., and Dorsey, R.J., 2022, Oligocene onset of uplift and inversion of the Cascadia forearc, southern Oregon Coast Range, USA: Geology, v. 50, p. 603–609.

EXPANDED METHODS

Sample Preparation & Mineral Separation

Detrital zircon were separated from 22 consolidated bedrock samples (~3–5 kg each) and three samples of unconsolidated modern river sand (~10–15 kg each) using standard procedures of crushing, sieving, and density and magnetic separation at the Mineral Separation Laboratory at Northern Arizona University by M. Darin. Most bedrock samples are composed of fine to medium sand (125–500 µm), although few samples (18COA-2, 18COA-6, 19COA-1, 19COA-2, 19COA-5, and 19COA-6) were as fine as coarse silt to very fine sand (31–150 µm). Special care was taken throughout the sampling and preparation process to avoid and minimize risks of contamination both in the field and lab, and to maintain consistency in the processing of all samples in this study.

Bedrock samples were first cleaned with compressed air to remove loose and potentially foreign material from their surfaces. Samples were then comminuted in a jaw crusher to reduce the size to < 20 mm, and next in a roller mill to further reduce their size to < 2 mm. The resultant sand was dry sieved using a 500-µm (no. 35) stainless steel sieve, and material that passed the filter (≤ 500 µm) was maintained for the next steps; material ≥ 500 µm was re-processed in the roller mill until the total volume of <500-µm sand was ~2.4–2.7 L. Unconsolidated modern river

samples were only subject to dry sieving to ≤ 500 µm, and 9.0–15.0 L of sand was reserved for further processing.

Density and magnetic separation procedures are rather effective at isolating zircon minerals due to its relatively high density (~4.7 g/cm^3) and generally non-magnetic properties (if inclusion-free). All samples were processed on a Gemeni water table to remove the lowest density minerals and fine silt. Upon completion, the heaviest fraction of grains were decanted and transferred to aluminum foil containers and dried in a ~100°C oven for ~15–50 hours. Once completely dry, a ~70–140 mL of split of sand was processed with a hand magnet to remove the most magnetic minerals from the sample. The remaining material was then submerged in methylene iodide (CH_2I_2; standard density = 3.32 g/cm^3), and gently stirred several times and left alone for ~20–30 minutes to allow heavier minerals to sink. The "light" fraction that floats was cleaned and discarded, and the sunken or "heavy" fraction was thoroughly cleaned with acetone, dried under a heat lamp, and preserved. The heavy fraction was then processed using a Frantz Isodynamic Magnetic Separator at discrete steps of 0.3, 0.8, 1.3, and 1.8 A. After these steps, the non-magnetic fraction was viewed under a binocular scope to assess zircon quality and abundance and is then transferred to a paper packet for mounting. Zircon were not hand-picked prior to mounting in order to avoid introducing bias toward more euhedral, large, or younger grains that appear less colored than older grains with greater radiation damage.

For detrital analyses, a large split of grains (generally thousands of grains) was incorporated into a 1" epoxy mount together with fragments or loose grains of Sri Lanka, FC-1, and R33 zircon crystals that are used as primary standards. For the one igneous sample (18COA-6), ~50 high-quality grains were selected and mounted with standards. All mounts were sanded down to a depth of ~20 microns, polished, cleaned, and imaged prior to isotopic analysis using a

Hitachi 3400N SEM and a Gatan CL2 detector system (www.geoarizonasem.org) to provide a guide for locating analysis pits in optimal locations. Back-scattered Emission (BSE) images were made for all sample mounts and several samples (18COA-6, 19COA-1, 19COA-2, 20COA-21, 20COA-22) were supplemented with cathodo-luminescence (CL) images.

U-Pb Analytical Methods

U-Pb geochronological analysis of zircon grains was conducted by high-resolution laser-ablation inductively-coupled-plasma mass spectrometry (HR LA-ICPMS) at the Arizona LaserChron Center (Gehrels et al., 2006, 2008; Gehrels and Pecha, 2014). Between 50 and 525 (n_{mean} = 283) unpicked (random) zircon grains were analyzed from each sample. Analyses involve ablation of zircon with a Photon Machines Analyte G2 excimer laser equipped with HelEx ablation cell using a spot diameter of 20 microns. The ablated material is carried in helium into the plasma source of a ThermoFisher Element2 single-collector high-resolution ICPMS, which sequences rapidly through U, Th, and Pb isotopes.

Signal intensities are measured with an SEM that operates in pulse counting mode for signals less than 50K cps, in both pulse-counting and analog mode for signals between 50K and 5M cps, and in analog mode above 5M cps. The calibration between pulse-counting and analog signals is determined line-by-line for signals between 50,000 and 5,000,000 cps, and is applied to >5,000,000 cps signals. Four intensities are determined and averaged for each isotope, with dwell times of 0.0052 sec for 202, 0.0075 sec for 204, 0.0202 sec for 206, 0.0284 sec for 207, 0.0026 sec for 208, 0.0026 sec for 232, and 0.0104 sec for 238.

With the laser set to an energy density of ~5 J/cm^2, a repetition rate of 8 hz, and an ablation time of 10 seconds, ablation pits are ~12 µm in depth. Sensitivity with these settings is approximately ~5,000 cps/ppm. Each analysis consisted of 5 seconds on peaks with the laser off

(for backgrounds), 10 seconds with the laser firing (for peak intensities), and a 20-second delay to purge the previous sample and save files.

Data Reduction

AgeCalcML Software

Following analysis, data reduction was performed using AgeCalcML (version 1.42), an open-source software platform with a MATLAB-based graphical user interface (GUI) developed at the Arizona LaserChron Center by Kurt Sundell (now at Idaho State University). This program is used for reducing, visualizing, and reporting single mineral U-Th-Pb, Lu-Hf, and trace element data generated by single-collector and multi-collector LA-ICP-MS. The open-source code and standalone GUI incorporate the same community-established protocols developed for the original Excel-based AgeCalc (Gehrels et al., 2008; Horstwood et al., 2016) and can be adapted to other LA-ICP-MS laboratories with laboratory-specific protocols. Additional information about AgeCalcML can be found on the web (https://www.kurtsundell.com/agecalcml). The source code and latest releases can be found on GitHub (github.com/kurtsundell/AgeCalcML).

Data Filtering & Discordance Criteria

Data reduction and visualization procedures primarily follow the recommendations of Spencer et al. (2016) and Vermeesch (2021a). Critically, and unlike many recent DZ studies, we chose not to implement an arbitrary discordance filter to the raw data. We instead follow the recommendations of Vermeesch (2021a) and use his "concordia distance" (d_c) criterion to evaluate $^{206}Pb/^{238}U$ vs. $^{207}Pb/^{235}U$ age discordance for most analyses. The "Stacey-Kramers cutoff" (d_{sk}) criterion was used for only tuff (18COA-6) and modern river sand samples (20COA-1, 20COA-2, 20COA-24) based on observed horizontal Discordia arrays in these samples that likely reflect low-temperature hydrothermal alteration of primary zircon derived from the Cascades Arc. Despite the inherent difficulties in measuring the low concentrations of ^{207}Pb in young (< 400 Ma) zircon

(Spencer et al., 2016; and references therein), we apply the same discordance criterion to all grains because a young discordant grain suffers the same ambiguity as an older discordant grain as to exactly 'where' it left concordia (Mezger and Krogstad, 1997; Vermeesch, 2021a).

In order to produce a minimally filtered dataset with only a nominal ^{204}Pb-correction, the following filter settings were applied for all samples and analyses in AgeCalcML. First, in the 'Session Details' window, 'ACF corrections for standards' were set as follows:

- Check all (Use Avg ACF, FC1, SL, and R33), but leave "Use 235?" unchecked, and then run the following:
- ACF Correction ^{238}U: select "Minimize Offset"
- ACF Correction Low-int ^{206}Pb: select "Minimize Offset"

Next, each filter value in the 'Data Filter' window was prescribed as follows:

- 6/8 vs 6/7 Best Age (Ma) = 1200 – *disregarded later for concordia age (see below)*
- 6/8 uncert cutoff (%) = 10
- 6/7 uncert cutoff (%) = 10
- Discordance cutoff (Ma) = 2400 – *effectively <u>no</u> discordance cutoff applied*
- Discord filter (%) = 100 – *allows all analyses to pass, up to 100% discordant*
- Rev discord. Filter (%) = 1000 – *allows all reverse discordant analyses to pass*
- 204Pb filter (cps) = 600
- 206/204 factor = 5 – *applies a low or conservative common-Pb correction*
- 6/8 OD (overdispersion) factor = 0.6
- 6/7 OD (overdispersion) factor = 1.0
- Reject STD (%) = 20
- "Reject STD?" = checked

Once the reduction parameters are set, data reduction is performed by AgeCalcML that:

1) Decodes .dat files from the Thermo software such that individual intensities for measurement are available (routine written by John Hartman, University of Arizona).

2) Imports intensities and a sample name for each analysis.

3) Calculates average intensities for each isotope (based on the sum of all counts while the laser is firing).

4) Subtracts ^{204}Hg from the 204 signal to yield ^{204}Pb intensity (using natural ^{202}Hg/^{204}Hg of 4.3). This Hg correction is not significant for most analyses because our Hg backgrounds are low (generally ~150 cps at mass 204).

5) Performs a common Pb correction based on the measured ^{206}Pb/^{204}Pb, the assumed composition of common Pb based on Stacey and Kramers (1975), and the user-defined input for the "206/204 factor" (see above).

6) Calculates measured 206/238, 206/207, and 208/232 ratios.

7) Compares measured and known ratios for the three standards to determine fractionation factors for 206/238, 206/207, and 208/232. These correction factors are generally <5% for 206/238, <2% for 206/207, and <20% for 208/232.

8) Uses a sliding-window average to apply fractionation factors to unknowns (generally averaging 8 standard analyses).

9) Calculates fractionation-corrected 206/238, 206/207, and 208/232 ratios and ages for unknowns.

10) Propagates measurement uncertainties for 206/238 and 208/232 that are based on the scatter about a regression of measured values. Uncertainties for 206/207 and 206/204 are based on the standard deviation of measured values since these ratios generally do not

change during an analysis. The sum of this uncertainty and any overdispersion factor is reported as the internal (or measurement) uncertainty for each analysis. These uncertainties are reported at the 1σ level.

11) Calculates the down-hole slope of 206/238 to highlight analyses in which 206/238 is compromised due to heterogeneity in age (e.g., crossing an age boundary) or intersection of a fracture or inclusion.

12) Calculates concentrations of U and Th for unknowns based on the measured intensity and known concentrations of FC-1.

13) Calculates the external (systematic) uncertainties for 206/238, 206/207, and 208/232, which include contributions from (a) the scatter of standard analyses, (b) uncertainties in the ages of the standards, (c) uncertainties in the composition of common Pb, and (4) uncertainties in the decay constants for ^{235}U and ^{238}U.

14) Determines a "Best Age" for each analysis, which is generally the 206/238 age for dates less than than the user-defined "6/8 vs 6/7 Best Age (Ma)" input, and the 206/207 age for dates greater than it.

15) Corrects $^{206/238}$U ages for U-Th disequilibrium. This has a significant impact only on very young (~<2 Ma) ages.

16) Calculates the radiation dosage that the analyzed portion of each zircon has experienced, assuming a value of 2.3 for the Th/U of the magma. This is plotted against 206/238 age to help identify Pb loss.

The reduced datasets were then exported as a 'Data Table' and additional data were added to each (File DR2). First, 'Best Age' and errors in the output AgeCalcML table are replaced with

the concordia age, which represents a kind of weighted mean between the individual U-Pb chronometers (^{206}Pb/^{238}U, ^{207}Pb/^{235}U, ^{207}Pb/^{206}Pb) and offers the best precision of all (Ludwig, 1998; Vermeesch, 2021a). Concordia ages were calculated using the online version of IsoplotR (Vermeesch, 2018) with the following parameters prescribed under the "ages" Options Menu:

- Input errors = 1se (%)
- Input format = [07/35], [06/38]
- NO disequilibrium correction
- ^{238}U/^{235}U ratio = 137.818 ± 0.0225
- ^{238}U decay constant = 0.000155125 ± 8.3e^{-8} Myr^{-1}
- ^{235}U decay constant = 0.00098485 ± 6.7e^{-7} Myr^{-1}
- NO common Pb correction (*except for samples 20COA-1, 20COA-2, and 20COA-24, for which a* "Stacey-Kramers" *common-Pb correction was applied*)
- Show Discordance = before comm Pb corr (if any)
- Discordance Type = 'concordia distance' or 'Stacey-Kramers cutoff' *(see above)*
- Sig figs = 3

Before exporting the final reduced data tables (see File DR2), we also calculate the effective uranium (eU) concentration for each analysis using the following equation: eU = U + (Th*0.235). Lastly, for ease of interpretation and evaluation of results, zircon analyses were qualified in the 'Age Class' field following the recommended scheme of Spencer et al. (2016):

- Y = youngest concordant detrital or igneous analysis
- I = igneous/magmatic grain; age likely reflects primary magmatic crystallization
- S = other detrital grain; age overlaps concordia within 2σ
- D = outside discordance threshold, does not overlap concordia within 2σ, or age information regarded as geologically meaningless
- P = interpreted to have undergone radiogenic-Pb loss based on high eU (≥1000 ppm)

- ▪ M = metamorphic grain with potential Pb-loss based on high U/Th (≥ 10)

- ▪ X = inherited/xenocrystic grain (unreliable for eruption age)

- ▪ [blank] = 'Age Class' undetermined

Data Visualization and Age Determinations

All concordia, weighted mean, and radial age plots (Figs. DR2–DR4) were generated were calculated using IsoplotR (Vermeesch, 2018). Age probability diagrams of DZ data including cumulative density functions (CDF) and kernel density estimates (KDE) were plotted using the detritalPy toolset (Sharman et al., 2018). All maximum and true depositional age estimates reported in Table 1 were calculated using IsoplotR (Vermeesch, 2018) and by one of three methods: (1) the 'youngest single concordant grain' (YSCG; Dickinson and Gehrels, 2009; Copeland, 2020); (2) the 'maximum likelihood age' (MLA), a purely statistical estimate that converges to the actual or 'true' depositional age (TDA) with increasing sample size (Vermeesch, 2021b); and (3) the youngest cluster of three or more dates whose ages overlap within 2σ error (YC2σ), identical to the 'YC2σ(3+)' method of Dickinson and Gehrels (2009). The youngest dates from each sample are plotted in Figures DR2–DR4. Dates are only excluded from these estimates if they either: (1) do not overlap concordia within 2σ analytical uncertainty (Spencer et al., 2016); or (2) have unusually high eU (> 1000 ppm) or U/Th (> 10), which indicates a susceptibility to radiation damage and enhanced potential for lead loss (Mezger and Krogstad, 1997; Marsellos and Garver, 2010).

Following the nominal common-lead correction applied in the data reduction steps outlined above, an additional [204]Pb-correction was applied only to DZ to the three modern river samples (20COA-1, 20COA-2, 20COA-24) and the Empire tuff sample (18COA-6), which display minor but systematic horizontal discordia arrays indicative of common-lead contamination (Anderson et

al., 2019). For these samples, discordance was evaluated using the Stacey-Kramers criterion (Stacey and Kramers, 1975); for all other detrital samples, discordance was evaluated using the concordia distance (d_c) criteria (Vermeesch, 2021a).

SUPPLEMENTAL FIGURES
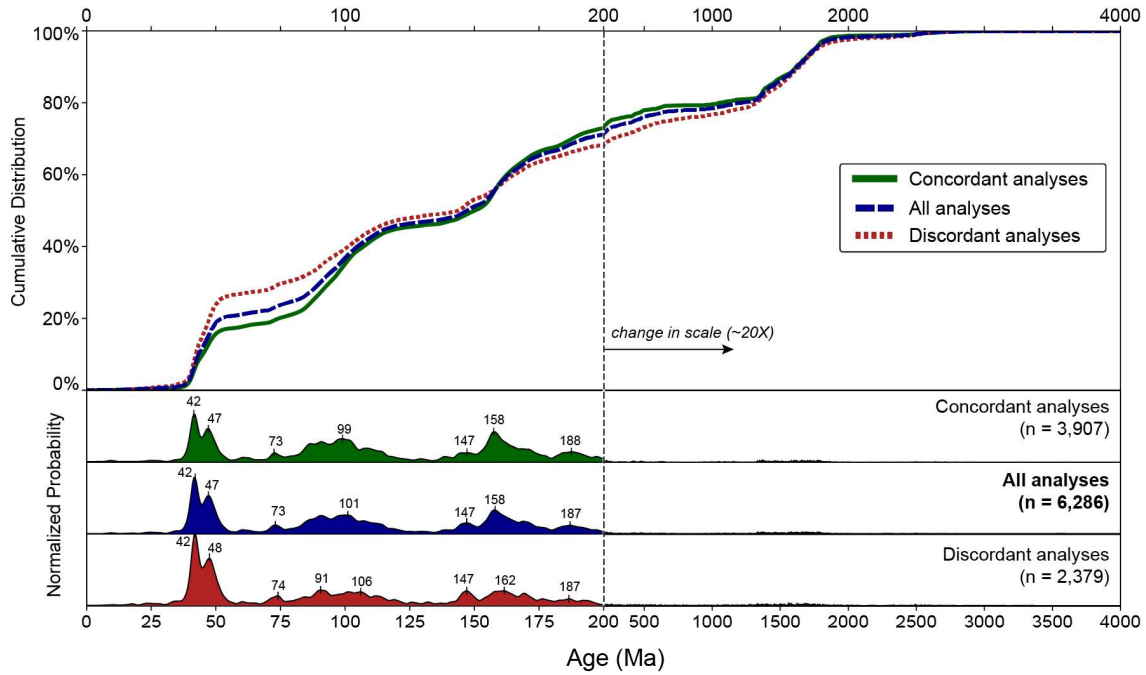
Figure DR1. Comparison of concordant and discordant detrital zircon (DZ) U-Pb analyses from all bedrock DZ samples shown in Table 1 except for tuff sample 18COA-6 (n=38) from the Empire Formation. Cumulative (top) and normalized relative (bottom) age distributions are plotted as kernel density estimates (KDE) with optimized fixed bandwidths (Sharman et al., 2018); note the change in scale at 200 Ma. The strong similarity between the concordant and discordant age distributions indicates that discordance is independent of age such that all dominant age modes and probabilities are represented in the concordant data, as shown in Figure 2.
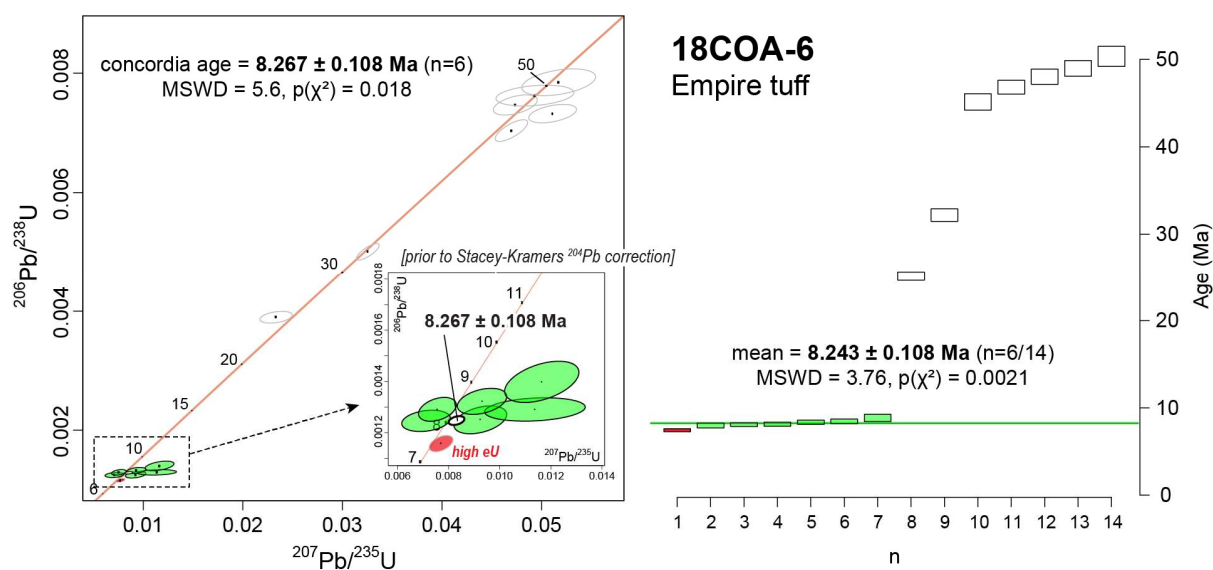
Figure DR2. Wetherill concordia diagram (left) and weighted mean age plot (right) for Empire tuff sample 18COA-6. All errors are displayed at 2σ, and only a subset of the youngest group of analyses are shown in each plot. Data outlined in gray are excluded from concordia and weighted mean age estimates. The red data point was also excluded from age estimates due to its unusually high eU concentration (4,087 ppm). The weighted mean age estimate of 8.243 ± 0.108 Ma is interpreted as the eruption age, or true depositional age (TDA), of the Empire tuff. MSWD = mean square of weighted deviates.
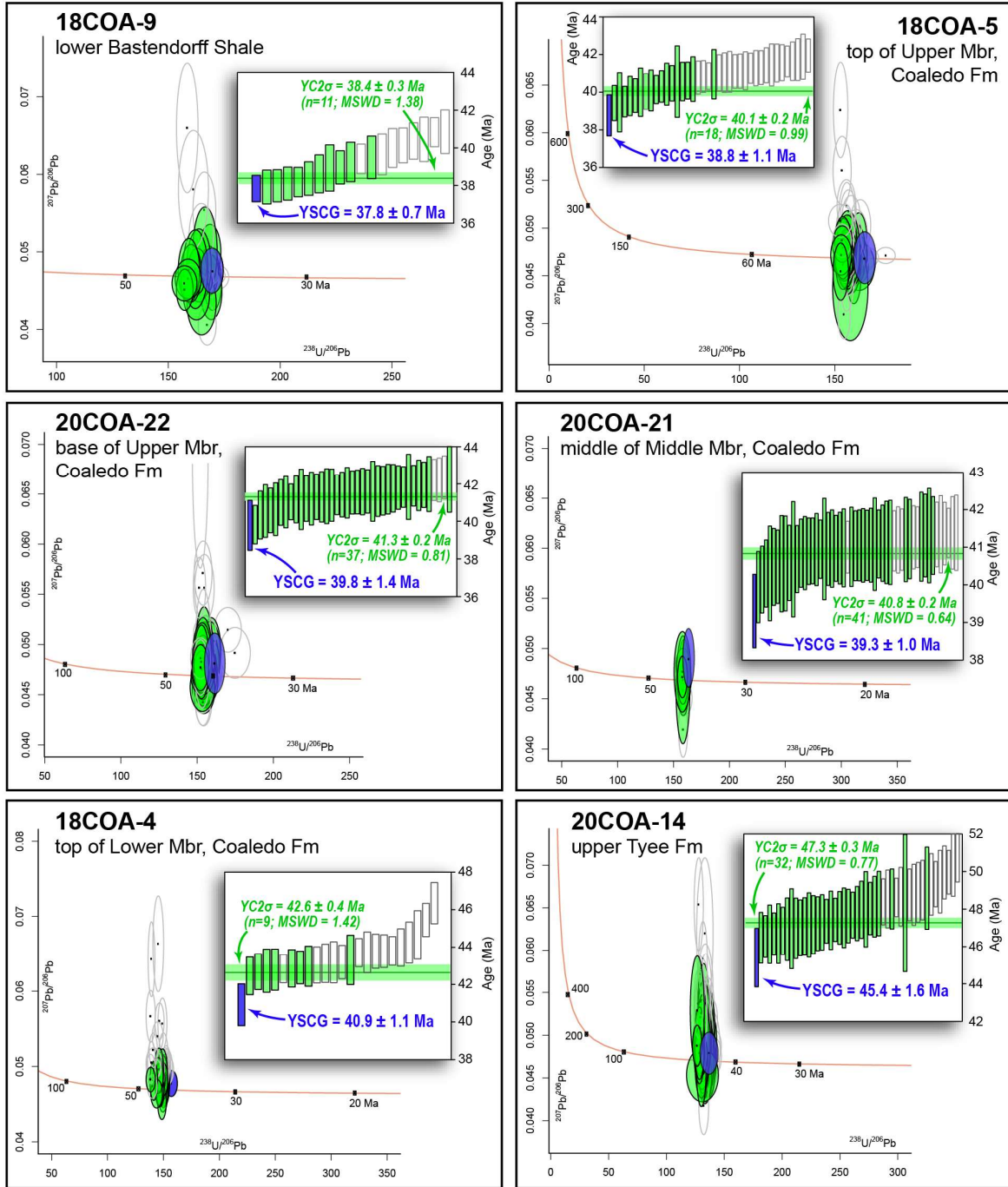
Figure DR3. Terra-Wasserburg U-Pb concordia and weighted mean age plots (inset) for bedrock detrital zircon samples that contain abundant (≥10%) near-depositional-age dates (see Table 1). All errors are displayed at 2σ, and only a subset of the youngest group of analyses are shown in each plot. For each sample, the youngest single concordant grain (YSCG) is shown in blue and is interpreted as the true depositional age (TDA) of the stratum; see text for discussion. Analyses in blue and green were used to estimate the maximum depositional age (MDA) from the youngest cluster of three or more concordant grains overlapping within ±2σ error (YC2σ). Analyses outlined in gray do not overlap concordia or contain high eU (≥1000 pm) or Th/U (≥10) and are excluded from depositional age estimates. MSWD = mean square of weighted deviates.
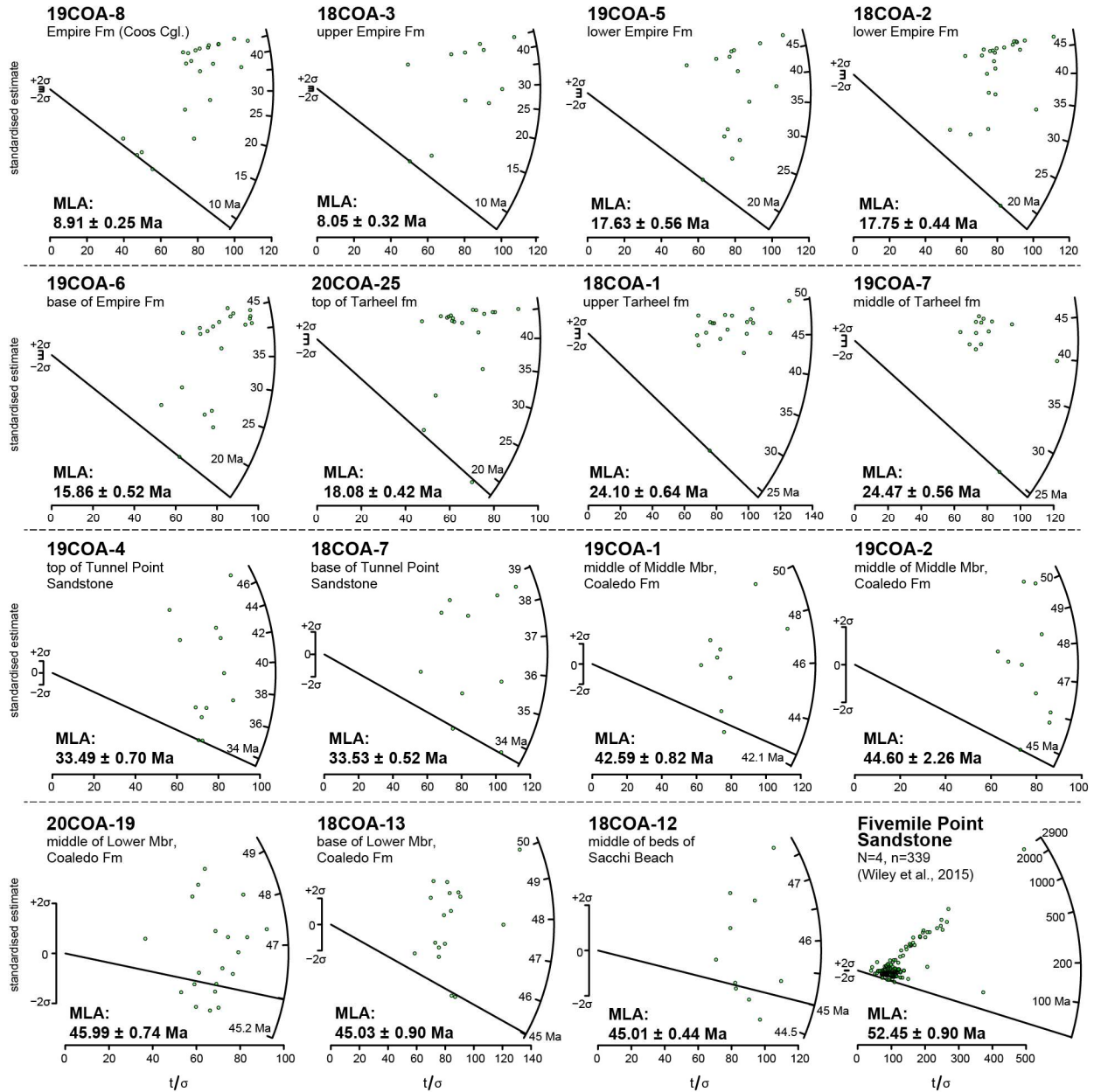
Figure DR4. Radial plots of bedrock detrital zircon samples that contain few (<10%) near-depositional-age dates (see Table 1). All errors are reported at 2σ. Only a subset of the youngest group of analyses are shown in each plot, except for the Fivemile Point Sandstone samples (N) which are compiled from Wiley et al. (2015) and shows all analyses (n) reported therein. For all samples shown, the minimum age model or "Maximum Likelihood Age" (MLA) of Vermeesch (2021b) is interpreted as the maximum depositional age of the stratum.
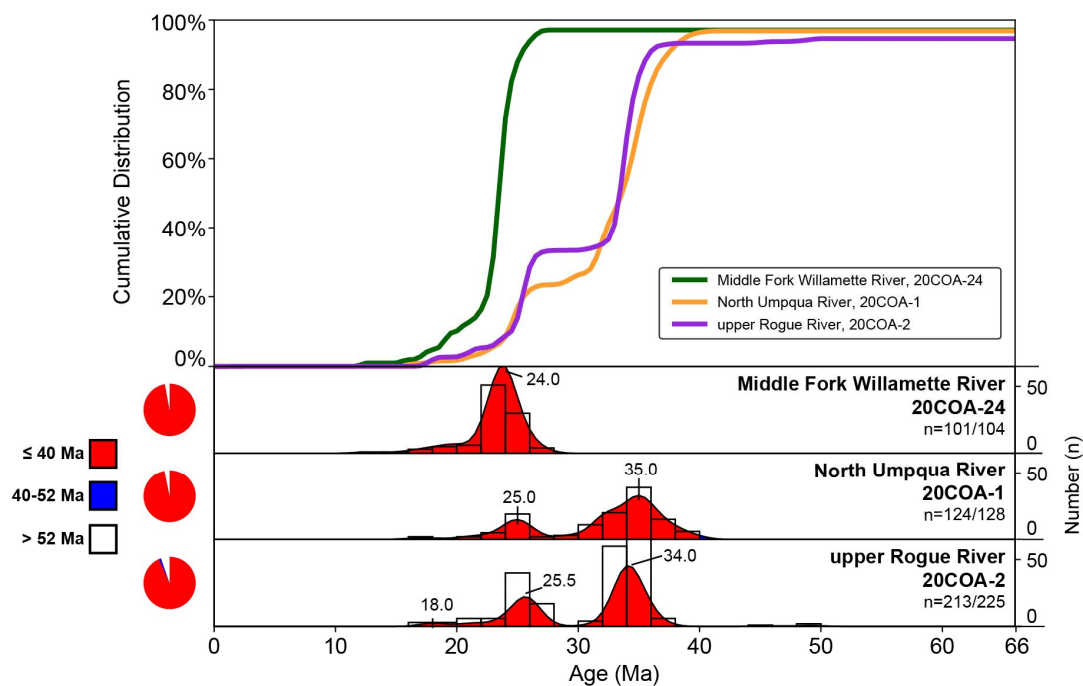
Figure DR5. Detrital zircon U-Pb age data from modern river samples in this study. Cumulative (top) and normalized relative probability density functions (bottom) are displayed as kernel density estimates (KDE) with optimized fixed bandwidths (Sharman et al., 2018). Plots are cut off at 66 Ma to emphasize the majority of data (>95%), whereas pie plots depict the entire dataset including ages >66 Ma. Sample locations are shown in Figure 1 and include: sample 20COA-24 from the Middle Fork of the Willamette River (44.022522°N, 122.950171°W); sample 20COA-1 from the North Umpqua River (43.332901°N, 123.005989°W); and sample 20COA-2 from the upper Rogue River (42.592688°N, 122.822058°W).
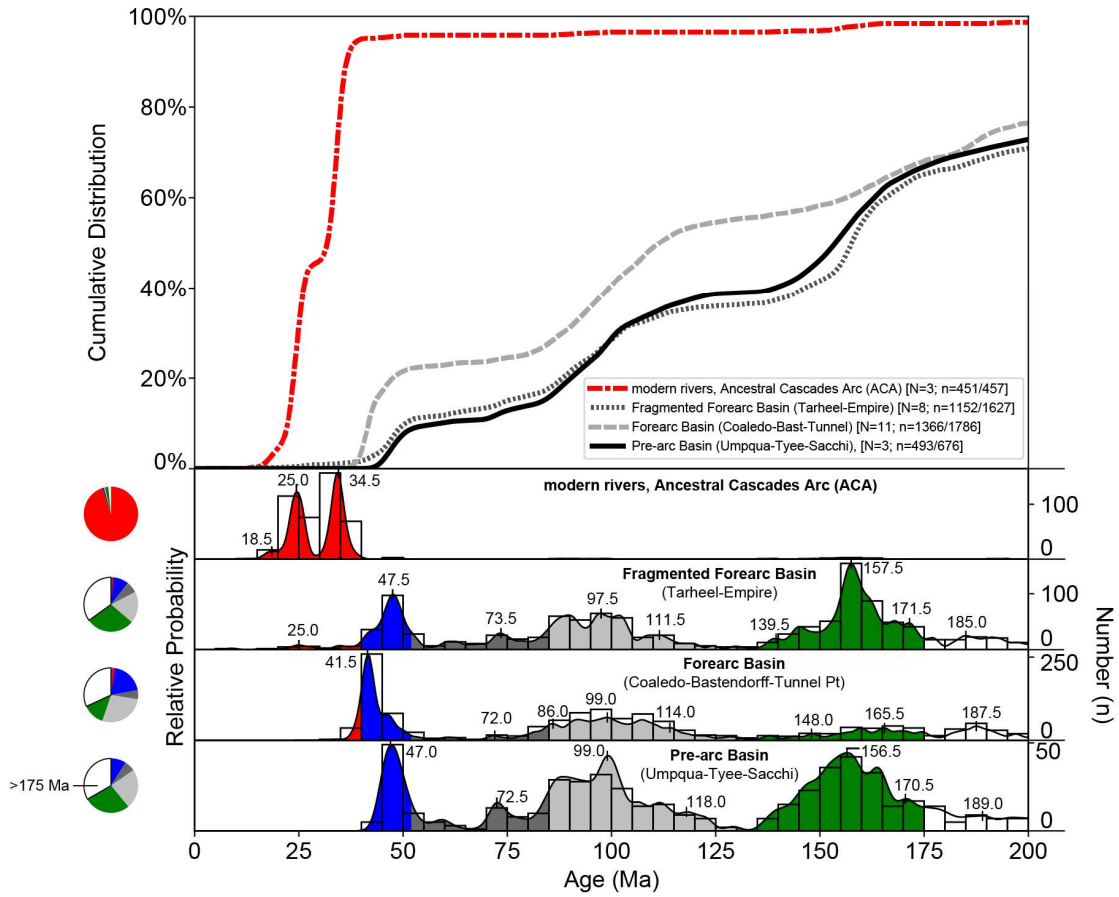
Figure DR6. Concordant detrital zircon (DZ) U-Pb age analyses (n), with samples (N) grouped into a middle Eocene 'Pre-arc Basin' stage, a late Eocene to Oligocene 'Forearc Basin' stage, and a Miocene 'Fragmented Forearc Basin' stage; the latter excludes Empire tuff sample 18COA-6. Cumulative (top) and normalized relative (bottom) age distributions are plotted as histograms and kernel density estimates (KDE) with optimized fixed bandwidths (Sharman et al., 2018). The strong similarity between the composite Pre-arc and Fragmented Forearc age spectra supports our hypothesis that the Miocene Tarheel and Empire formations contain a significant component of second-cycle Klamath Mountains (175–130 Ma) and Clarno-Challis (52–40 Ma) detritus recycled from the thick undelrying middle Eocene succession (i.e., Tyee, Sacchi Beach and Coaledo formations).

REFERENCES CITED IN THIS DATA REPOSITORY FILE ONLY

Copeland, P., 2020, On the use of geochronology of detrital grains in determining the time of deposition of clastic sedimentary strata: Basin Research, v. 32, no. 6, p. 1532–1546, https://doi.org/10.1111/bre.12441.

Dickinson, W. R., and Gehrels, G. E., 2009, Use of U–Pb ages of detrital zircons to infer maximum depositional ages of strata: a test against a Colorado Plateau Mesozoic database: Earth and Planetary Science Letters, v. 288, no. 1–2, p. 115–125, https://doi.org/10.1016/j.epsl.2009.09.013.

Gehrels, G.E., Valencia, V., and Pullen, A., 2006, Detrital zircon geochronology by Laser-Ablation Multicollector ICPMS at the Arizona LaserChron Center, *in* Loszewski, T., and Huff, W., eds., Geochronology: Emerging Opportunities, Paleontology Society Short Course: Paleontology Society Papers, v. 11, 10 p.

Gehrels, G. E., Valencia, V. A., and Ruiz, J., 2008, Enhanced precision, accuracy, efficiency, and spatial resolution of U-Pb ages by laser ablation–multicollector–inductively coupled plasma–mass spectrometry: Geochemistry, Geophysics, Geosystems, v. 9, no. 3, 13 p., https://doi.org/10.1029/2007GC001805.

Gehrels, G. and Pecha, M., 2014, Detrital zircon U-Pb geochronology and Hf isotope geochemistry of Paleozoic and Triassic passive margin strata of western North America: Geosphere, v. 10, no. 1, p. 49–65.

Horstwood, M.S., Košler, J., Gehrels, G., Jackson, S.E., McLean, N.M., Paton, C., Pearson, N.J., Sircombe, K., Sylvester, P., Vermeesch, P. and Bowring, J.F., 2016. Community-derived standards for LA-ICP-MS U-(Th-) Pb geochronology–Uncertainty propagation, age interpretation and data reporting: Geostandards and Geoanalytical Research, v. 40, no. 3, p. 311–332.

Ludwig, K.R., 1998, On the treatment of concordant uranium-lead ages: Geochemica et Cosmochima Acta, v. 62, p. 665–676, https://doi.org/10.1016/S0016-7037(98)00059-3.

Marsellos, A.E., and Garver, J.I., 2010, Radiation damage and uranium concentration in zircon as assessed by Raman spectroscopy and neutron irradiation: American Mineralogist, v. 95, no. 8–9, p. 1192–1201.

Mezger, K., and Krogstad, E.J., 1997, Interpretation of discordant U-Pb zircon ages: An evaluation: Journal of Metamorphic Geology, v. 15, no. 1, p. 127–140.

Sharman, G. R., Sharman, J. P., and Sylvester, Z., 2018, detritalPy: A Python-based toolset for visualizing and analyzing detrital geo-thermochronologic data: Depositional Record, v. 4, p. 202–215, https://doi.org/10.1002/dep2.45.

Spencer, C. J., Kirkland, C. L., and Taylor, R. J., 2016, Strategies towards statistically robust interpretations of in situ U–Pb zircon geochronology: Geoscience Frontiers, v. 7, no. 4, p. 581–589, https://doi.org/10.1016/j.gsf.2015.11.006

Stacey, J.S., and Kramers, J.D., 1975, Approximation of terrestrial lead isotope evolution by a two stage model: Earth and Planetary Science Letters, v. 26, p. 207–221.

Vermeesch, P., 2018, IsoplotR: A free and open toolbox for geochronology: Geoscience Frontiers, v. 9, no. 5, p. 1479–1493, https://doi.org/10.1016/j.gsf.2018.04.001.

Vermeesch, P., 2021a, On the treatment of discordant detrital zircon U–Pb data: Geochronology, v. 3, no. 1, p. 247–257, https://doi.org/10.5194/gchron-3-247-2021.

Vermeesch, P., 2021b, Maximum depositional age estimation revisited: Geoscience Frontiers, v. 12, no. 2, p. 843–850, https://doi.org/10.1016/j.gsf.2020.08.008.

Wiley, T.J., McClaughry, J.D., Niewendorp, C.A., Ma, L., Herinclx, H.H., and Mickelson, K.A., 2015, Geologic map of the southern Oregon coast between Bandon, Coquille, and Sunset Bay, Coos County, Oregon: Oregon Department of Geology and Mineral Industries, Open File Report 0-15-04, 57 p., 4 plates.